Synthesis, Characterization and Comparison of Photo-catalytic Efficiency of Fe3O4/SiO2/TiO2, SrFe12O19/SiO2/TiO2 and Fe3O4/SiO2/ZnO Core/shell/shell Nano-structures

Fatemeh Bavarsiha
Imam Khomeini International University Faculty of Engineering and Technology: Imam Khomeini International University Faculty of Technical and Engineering

Saeideh Dadashian
Biosphere Technology Company, Environmental Laboratory, Abhar, Iran

Mehdi Montazeri-Pour (montazeri.pour@bzte.ac.ir)
Buein Zahra Technical University https://orcid.org/0000-0001-5390-5039

Fardin Ghasemy-Piranloo
Biosphere Technology Company, Environmental Laboratory, Abhar, Iran

Masoud Rajabi
Imam Khomeini International University Faculty of Engineering and Technology: Imam Khomeini International University Faculty of Technical and Engineering

Research Article

Keywords: Photo-catalytic efficiency, Hard and soft magnetic composites, Core/shell/shell nanostructures, Magnetic properties

Posted Date: April 6th, 2021

DOI: https://doi.org/10.21203/rs.3.rs-384364/v1

Synthesis, Characterization and Comparison of Photo-catalytic Efficiency of $Fe_3O_4/SiO_2/TiO_2$, $SrFe_{12}O_{19}/SiO_2/TiO_2$ and $Fe_3O_4/SiO_2/ZnO$ Core/shell/shell Nano-structures

Fatemeh Bavarsiha[1,3], Saeideh Dadashian[1], Mehdi Montazeri-Pour[*2], Fardin Ghasemy-Piranloo[1], Masoud Rajabi[3]

[1] Biosphere Technology Company, Environmental Laboratory, Abhar, Iran

[2] Department of Chemical and Materials Engineering, Buein Zahra Technical University, Buein Zahra, Qazvin, Iran

[3] Department of Materials Science and Engineering, Faculty of Technology and Engineering, Imam Khomeini International University (IKIU), Qazvin, Iran

[*]Corresponding author: montazeri.pour@bzte.ac.ir ; montazerypor@ut.ac.ir

Abstract: In this research work, three magnetic composites of $Fe_3O_4/SiO_2/TiO_2$, $SrFe_{12}O_{19}/SiO_2/TiO_2$ and $Fe_3O_4/SiO_2/ZnO$ with core/shell/shell structures were successfully prepared by the sol-gel method. For this purpose, in the first step, soft magnetic and hard magnetic powders of Fe_3O_4 and $SrFe_{12}O_{19}$ were synthesized using carbon reduction and co-precipitation routes, respectively. In the second step, silica coating was performed by controlling the hydrolysis and condensation of the tetraethyl orthosilicate (TEOS) precursor on the magnetic cores. In the third step, a coating of TiO_2 or ZnO photo-catalytic shells was made on as-prepared composites using precursors of titanium *n*-butoxide (TNBT) or zinc nitrate hexahydrate, respectively. The as-prepared magnetically separable photo-catalysts were characterized using XRD, FESEM, TEM and VSM. The results of the FESEM and TEM analyses confirmed the formation of the core/shell/shell structures. The saturation magnetization of the $Fe_3O_4/SiO_2/TiO_2$, $SrFe_{12}O_{19}/SiO_2/TiO_2$ and $Fe_3O_4/SiO_2/ZnO$ photo-catalytic materials was 41.5 emu/g, 33 emu/g and 49 emu/g, respectively. Evaluation of the photo-catalytic activity of $Fe_3O_4/SiO_2/TiO_2$, $SrFe_{12}O_{19}/SiO_2/TiO_2$ and $Fe_3O_4/SiO_2/ZnO$ composites by using methylene blue (MB) shows degradation percentages of 84%, 80% and 58%, respectively, under UV illumination.

Keywords: Photo-catalytic efficiency, Hard and soft magnetic composites, Core/shell/shell nanostructures, Magnetic properties

1. Introduction

In recent years, the coating of particles surface by the different material and development of the core/shell structures have attracted considerable attention from scientific communities. Coating of core particles with a thin layer of a compatible material having different chemical composition can change the structure, size and

composition of particles; thereby it can control their magnetic, optical, mechanical, thermal, electrical and catalytic properties [1-3]. The nano-composites with core/shell structure can exhibit improved properties that are completely different relative to each of the core or shell materials [4]. Furthermore, this structure can simultaneously have the properties of core and shell materials. Multi-layered core/shell structures made up of a core and several shells around it have been attended recently [5].

Nowadays, due to increasing environmental concerns, many efforts have been conducted around the world to obtain effective materials and processes for the purification of contaminated water [6, 7]. Hence, purification processes of organic pollutants by using semiconductor nanoparticles such as ZnO, ZnS, TiO_2 and SnO_2, etc. have been studied [8-10]. In order to solve the problem of separation of photo-catalytic powders from purified water and allowing to be reusing them, TiO_2 and ZnO particles are coated on hard and soft magnetic powders to facilitate the separation of these photo-catalytic materials from the environment using an external magnetic field [11-13]. However, the photo-catalytic activity of TiO_2 and ZnO will be reduced in their direct contact with magnetic cores, which is due to the photo-dissolution phenomenon [14, 15]. In order to overcome this problem, three-layered core/shell/shell composites can be utilized. Thus, to prevent electrical contact and direct interaction between the magnetic core and the photo-catalytic shell, an intermediate SiO_2 shell can be applied between the magnetic core and the photo-catalytic shell [12, 16]. Typically, the Stöber method is used for the coating of the SiO_2 layer on the magnetic particles. Alcohol should be used as a reaction media [17-19]. This method involves the multi-stage hydrolysis and condensation of tetraethyl ortho-silicate (TEOS) in an alcoholic media in the presence of ammonia (NH_4OH) as a catalyst. The formation mechanism according to the reactions (1) and (2) can be described as:

$$Si(OC_2H_5)_4 + 4H_2O \rightarrow Si(OH)_4 + 4C_2H_5OH \quad (1)$$

$$Si(OH)_4 \rightarrow SiO_2 + 2H_2O \quad (2)$$

Reducing the concentration of TEOS in the solution will reduce particle size. Silica particles produced by this method are amorphous and porous. Similarly, the change in the concentration of ammonium hydroxide affects the size, porosity and shape of particles [20].

Fe_3O_4 is a natural ferrite, the most known and the oldest magnetic substance. The chemical formula of this material can be written as $FeO.Fe_2O_3$, which is similar to the spinel structure of $MgO.Al_2O_3$. $SrFe_{12}O_{19}$ is a hexagonal ferrite with a total chemical formula of $MO.6Fe_2O_3$ (M =Sr, Ba or Pb). Strontium hexaferrite as a ferri-magnetic material exhibits high coercive force, suitable chemical stability and low cost [21, 22].

In the present research, $Fe_3O_4/SiO_2/TiO_2$, $Fe_3O_4/SiO_2/ZnO$ and $SrFe_{12}O_{19}/SiO_2/TiO_2$ composites were synthesized. Magnetic properties of core/shell/shell photo-catalytic nanostructures having soft and hard magnetic cores, and photo-catalytic layers of TiO_2 and ZnO were investigated and compared. As far as the authors know, for the first time, the photo-catalytic activity of as-prepared composites has been examined and compared by the degradation of methylene blue dye under UV illumination.

2. Experimental

2.1. Materials

In this research work, zinc nitrate hexahydrate ($ZnNO_3.6H_2O$, Merck>99%), strontium chloride hexahydrate ($SrCl_2.6H_2O$, Merck, ≥ 99%), iron (III) chloride hexahydrate, ($FeCl_3.6H_2O$, Merck, > 99%), dimethyl-formamide (DMF, Merck>99.8%), absolute ethanol (C_2H_5OH, Merck, > 99.9%), ammonia solution (NH_4OH, 25 wt.%), sodium hydroxide (NaOH, Panreac AppliChem, > 98%), degreased carbon cotton, tetraethyl orthosilicate (TEOS, $C_8H_{20}O_4Si$, Merck, > 99%), hydroxypropyl cellulose (HPC, Sigma Aldrich), titanium n-butoxide (TNBT, Sigma-Aldrich, > 98%), isopropanol (C_3H_8O, Merck, > 99.5%) and deionized water were used throughout the experiments.

2.2. Synthesis of the magnetic cores

In this study, Fe_3O_4 magnetic particles and strontium ferrite particles were prepared using the carbon reduction and co-precipitation methods, respectively [23-25]. In order to obtain Fe_3O_4 particles, 80 g $FeCl_3.6H_2O$ was mixed into 150 ml of distilled water for 15 min. Subsequently, 7 g degreased carbon cotton was added to the solution, and it was subjected to the ultrasonic treatment for 10 min. Then, the product was collected and heated at 400 °C for 4 h.

To produce the strontium hexaferrite powder, at first $FeCl_3.6H_2O$ and $SrCl_2.6H_2O$ solutions were prepared in a mixture of distilled water/ethanol with a volume ratio of

1: 3. The molar ratio of Fe^{3+}/Sr^{2+} was 12 and the OH^-/Cl^- molar ratio was 2. The precipitate was filtered and washed. Then, it was placed in a dryer for 24 h under a temperature of 70°C. Finally, the dried powder was calcined at 950˚C temperatures for 1 h.

2.3. Coating of silica shell

Coating of silica shell on magnetic cores was done using the Stöber method. Fe_3O_4/SiO_2 nanostructures were fabricated as follows: At first, 0.05 g of Fe_3O_4 powder was dispersed into ethanol and distilled water with a ratio of 4 to 1 in an ultrasonic bath. Then, ammonia (25% by weight) and tetraethyl orthosilicate with a volume ratio of 8:1 were added to the mixture. The coated particles were separated from the suspension using a powerful magnet. Then obtained powder was washed with ethanol and distilled water and dried in a vacuum oven at 60 °C for 8 h.

In order to obtain the $SrFe_{12}O_{19}/SiO_2$ composite, 0.03 g of $SrFe_{12}O_{19}$ powder was dispersed under an ultrasonic bath in a mixture including isopropanol, distilled water, tetraethyl orthosilicate and ammonia solution with values of 250, 4, 1 and 0.15 ml, respectively [11]. The achieved powder was separated from the mixture using a strong magnet. Then, it was washed with isopropanol and distilled water and finally dried in a vacuum oven at 40 °C for 24 h.

2.4. Coating of photo-catalytic shells

In order to cover the ZnO photo-catalytic shell on core/shell particles, a solution of 0.6 g $ZnNO_3.6H_2O$ in 100 mL DMF was made and 0.05 g of the Fe_3O_4/SiO_2 powder was added to it. Then, the NaOH solution (0.02 M) was slowly added to the initial suspension and was placed under stirring for 6 h. The powders were separated from the solution using magnetic separation and washed with distilled water and ethanol several times, and dried in a dryer at 60 °C for 6 h. In the end, it was calcined at 500 °C for 2 h.

The Fe_3O_4/SiO_2 particles were coated by TiO_2 through the hydrolysis and condensation of titanium n-butoxide in ethanol solution. 0.03 g of the Fe_3O_4/SiO_2 particles, 0.24 ml distilled water, 0.1 g HPC and 60 ml absolute ethanol were kept under intense stirring. After dispersion, titanium n-butoxide and ethanol were added and kept for 90 minutes at 85°C. The obtained powder was washed several times by

using ethanol and distilled water and dried for 4 hours at 60°C. Finally, particles were calcined in an argon atmosphere at 500℃ for 2 h.

In another part of this study, 0.25 g of $SrFe_{12}O_{19}/SiO_2$ powder with ethanol (140ml) and distilled water (3ml) were dispersed in the ultrasonic bath for coating the TiO_2 photo-catalytic shell. Then a solution of titanium n-butoxide was added to the solution drop by drop and placed under stirrer at 90 °C for 2h. The composite was separated using magnetic separation and washed several times using water and ethanol. Then it was dried at 60°C for 6 h. In the end, it was calcined at 500°C for 1 h.

2.5. Study of photo-catalytic properties

In this study, the decomposition of methylene blue dye using UV light was used as a model for evaluation of the photo-catalytic properties. In this regard, the photo-catalytic powders were added to the methylene blue solution (50 mg/l). Afterwards, the as-prepared mixture was under a stirrer for 0.5 h in the dark and then it was exposed under the UV light. At specified intervals, the absorbance changes were obtained by an 1800 UV-Vis spectroscopy in the range of 500 to 800 nm.

2.6. Characterization

XRD (Philips PW1730) has been used to identify the phase composition of the samples. The morphology of the prepared composites was evaluated using a field emission scanning electron microscopy (FESEM, TE-SCAN Company, model MIRA3), and transmission electron microscopy (TEM, Philips model CM120 operating at 120 kV). Their magnetic properties were also analyzed by a vibrating sample magnetometer (VSM, Kavir Kashan Co., MDK6) at room temperature.

3. Results and discussion

Fig. 1 (a) and (b) show the X-ray diffraction patterns of the synthesized magnetic cores of the composite, $SrFe_{12}O_{19}$ and Fe_3O_4 powders, respectively. The $SrFe_{12}O_{19}$ single phase (JCPDS Card No. 1411-079) and the Fe_3O_4 single phase (JCPDS No. 19-0629) are obtained which are indicated by (●) and (■), respectively [23]. Fig. 1 (c), (d) and (e) show the X-ray diffraction patterns of the $SrFe_{12}O_{19}/SiO_2/TiO_2$, $Fe_3o_4/SiO_2/ZnO$ and $Fe_3o_4/SiO_2/TiO_2$ photo-catalytic composites with core/shell/shell structure, respectively. Due to the presence of the amorphous silica phase in three

composites, diffraction peaks for the silica phase were not observed. The TiO_2 Phase (JCPDS Card No. 1764-073) and the ZnO phase (JCPDS Card No. 36-1451) are indicated by the symbols (▲) and (▼), respectively [26-28]. By the comparison of the intensity of the photo-catalytic materials peaks in Fig. 1 (c) and (d), it is observed that the intensity of the peaks of the ZnO phase is much lower than that of the TiO_2 phases, although more time is taken for ZnO shell synthesis, which could be attributed to a more easy formation of the crystallized TiO_2 shell.

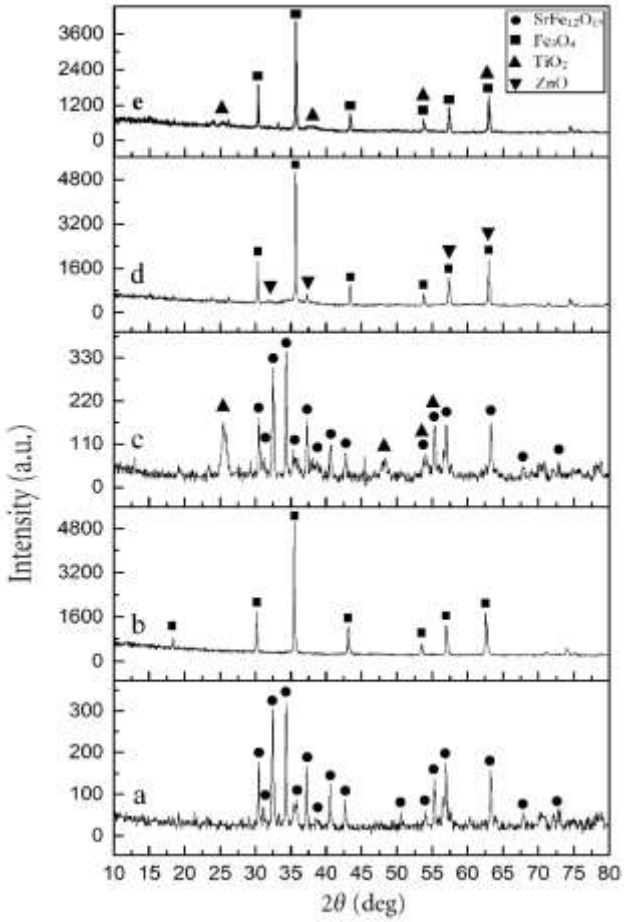

Fig. 1 XRD patterns of a) $SrFe_{12}O_{19}$ powder, b) Fe_3O_4 powder, c) $SrFe_{12}O_{19}/SiO_2/TiO_2$ composites, d) $Fe_3O_4/SiO_2/ZnO$ composites and e) $Fe_3O_4/SiO_2/TiO_2$ composites

Fig. 2 (a) and (e) show FESEM images of the Fe_3O_4 and $SrFe_{12}O_{19}$ powders, respectively. As shown in Fig. 2 (a), the Fe_3O_4 particles present the regular polygon structure, but $SrFe_{12}O_{19}$ particles have an irregular hexagonal structure. The average size of iron oxide (II, III) particles is approximately 350 nm, while the average size of strontium ferrite particles is 122 nm. Fig. 2 (b) and (f) show the FESEM images of the silica coating on magnetic particles of iron oxide (II, III) and strontium ferrite, respectively. The smooth coating around the magnetic particles confirms the

formation of SiO_2 shells. So, the coating of the SiO_2 shell on the magnetic particles is well done using the sol-gel method [18].

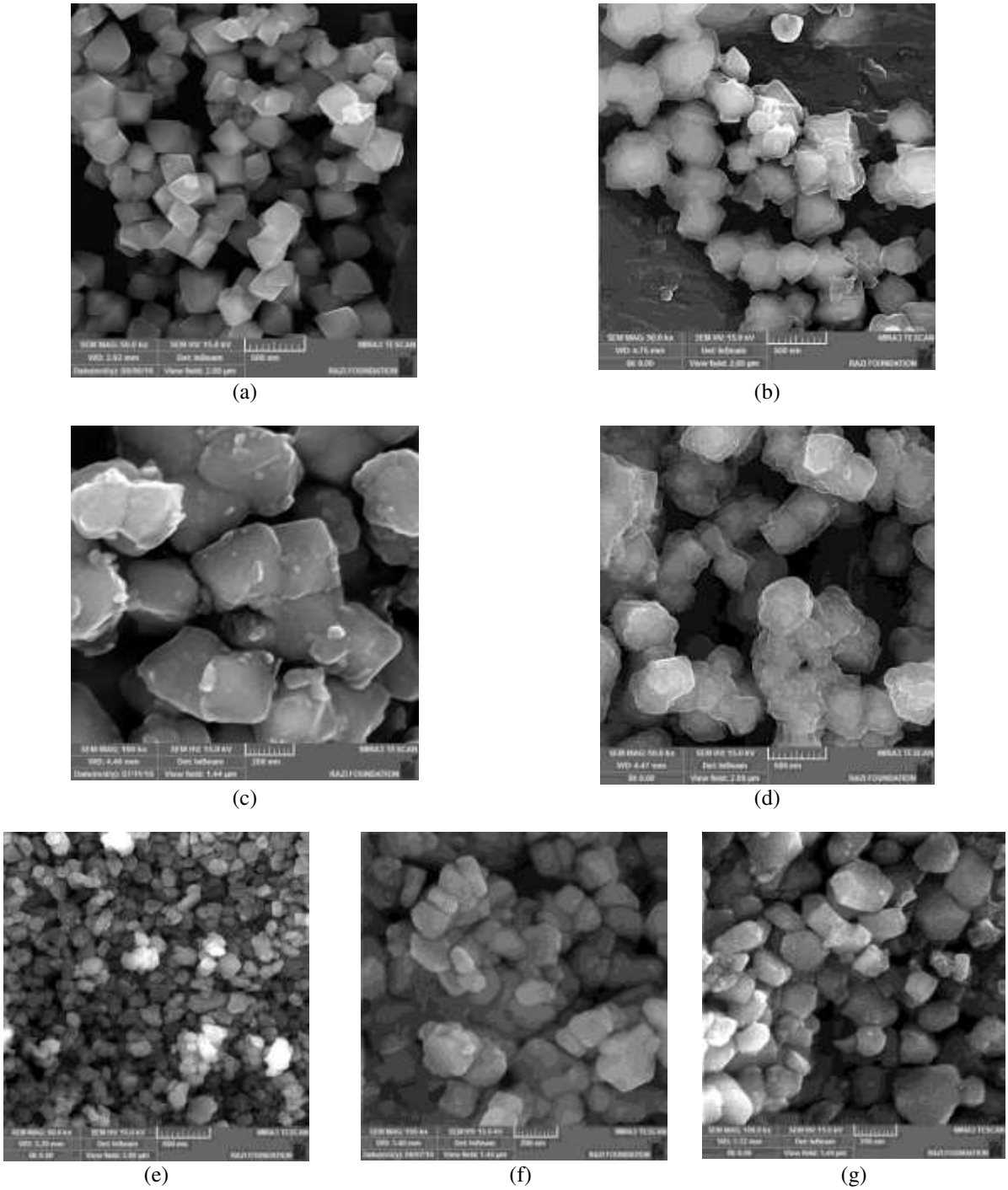

Fig. 2 FESEM micrographs of a) Fe_3O_4 powder, b) Fe_3O_4/SiO_2 composite, c) $Fe_3O_4/SiO_2/ZnO$ composite, d) $Fe_3O_4/SiO_2/TiO_2$ composite, e) $SrFe_{12}O_{19}$ powder, f) $SrFe_{12}O_{19}/SiO_2$ composite, and g) $SrFe_{12}O_{19}/SiO_2/TiO_2$ composite

Fig. 2 (c) shows the coating of the ZnO shell on the Fe_3O_4/SiO_2 composites. FESEM micrographs of TiO_2 shell coated on the Fe_3O_4/SiO_2 and the $SrFe_{12}O_{19}/SiO_2$ composites are displayed in Fig. 2 (d) and (g), respectively, which indicated that the photo-catalytic coating is uneven and its morphology is completely different from silica coating [26, 28, 29].

Also, EDX spectra of $Fe_3O_4/SiO_2/TiO_2$, $Fe_3O_4/SiO_2/ZnO$ and $SrFe_{12}O_{19}/SiO_2/TiO_2$ composites are exhibited in Fig. 3, based on which, the presence of Sr, Fe, Si, Ti, Zn and O elements in the prepared nanostructures has been confirmed. EDX results confirm the formation of $Fe_3O_4/SiO_2/ZnO$ and $SrFe_{12}O_{19}/SiO_2/TiO_2$ nanostructures in corresponding to other results [30, 31].

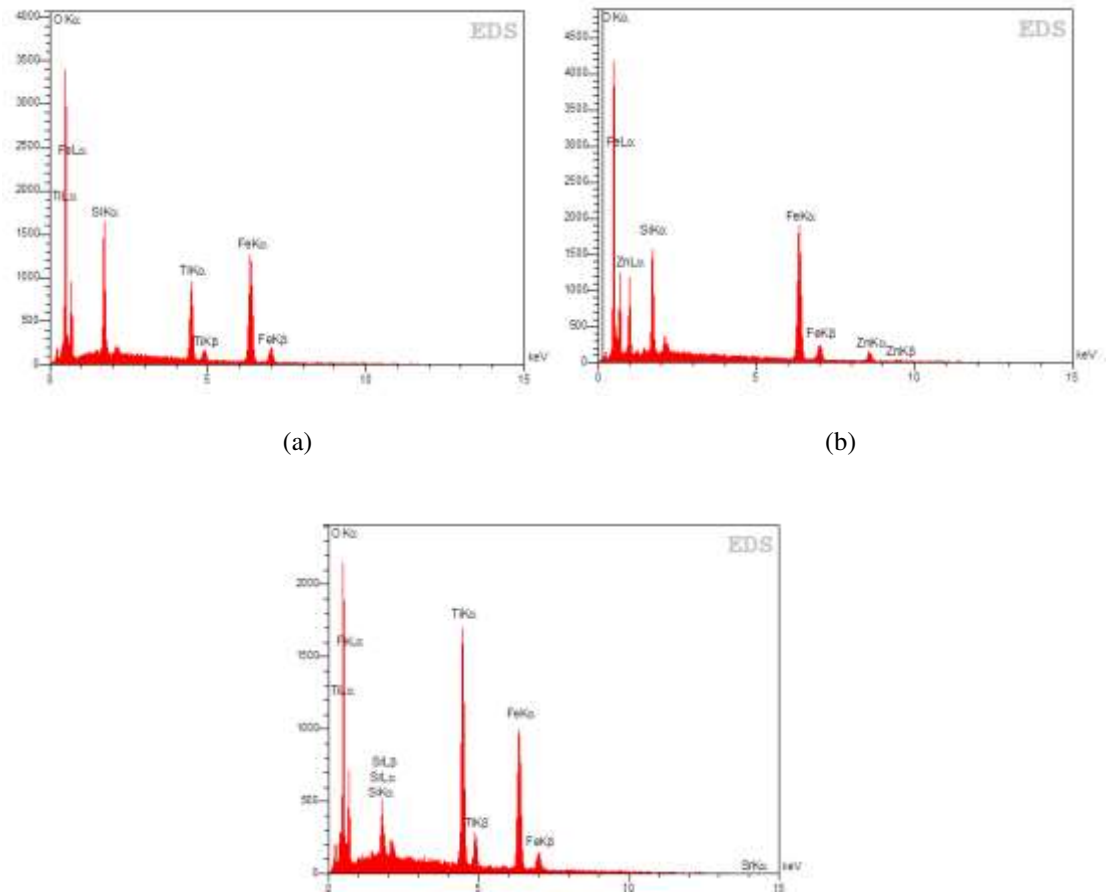

(a) (b)

(c)

Fig. 3 EDS spectra of the a) $Fe_3O_4/SiO_2/TiO_2$, b) $Fe_3O_4/SiO_2/ZnO$ and c) $SrFe_{12}O_{19}/SiO_2/TiO_2$ composites

The TEM images of $SrFe_{12}O_{19}/SiO_2$, $SrFe_{12}O_{19}/SiO_2/TiO_2$, Fe_3O_4/SiO_2, $Fe_3O_4/SiO_2/ZnO$ and $Fe_3O_4/SiO_2/TiO_2$ composites are shown in Figs. 4 (a), (b), (c), (d) and (e) respectively. As shown in Fig. 4 (a) and (c), a brighter shell surrounding the core particles is the silica coating. The more uniform coating formed on $SrFe_{12}O_{19}$ particles than that on the Fe_3O_4 particles could be attributed to the apparent shape of these core particles. The thickness of the SiO_2 shell has a significant effect on preventing of photo-dissolution phenomenon. In fact, the valence band of the magnetic cores is higher than that of the ZnO and TiO_2 and the conduction band of the magnetic cores is lower than that of the ZnO and TiO_2 which leads to the transfer of charge carriers from the ZnO and TiO_2 to the magnetic cores and the recombination of the electron-hole pair. Therefore, the life of the electron-hole is reduced. By the excessive reduction of the thickness of silica coating, the photo-catalytic efficiency of this composite is reduced. On the other hand, the high magnetic properties of the composites are important for better recovery. The excessive increase of the silica shell also results in a decrease in saturated magnetization and consequently, a reduction of retrieval ability of photo-catalytic particles by magnetic separation [14, 32]. In order to control the thickness of SiO_2 coating, the concentration of TEOS, water, alcohol, temperature and time of reaction are important factors [33, 34]. The thickness of the silica shell for soft and hard magnetic composites was approximately 15 and 20 nm. According to TEM observations, a thin coating of the TiO_2 and ZnO photo-catalytic particles is seen in Figs. 4 (b), (d) and (e), which obviously differ from the TEM micrographs of the SiO_2 shell in Figs. 4 (a) and (c). The ZnO layer formed on Fe_3O_4/SiO_2 is a few nanometer thick shells while the TiO_2 shells are more uniform which were formed at the lower times. The thickness of TiO_2 shells on $SrFe_{12}O_{19}$ and Fe_3O_4 particles has reached about 30 nm and 32 nm, respectively.

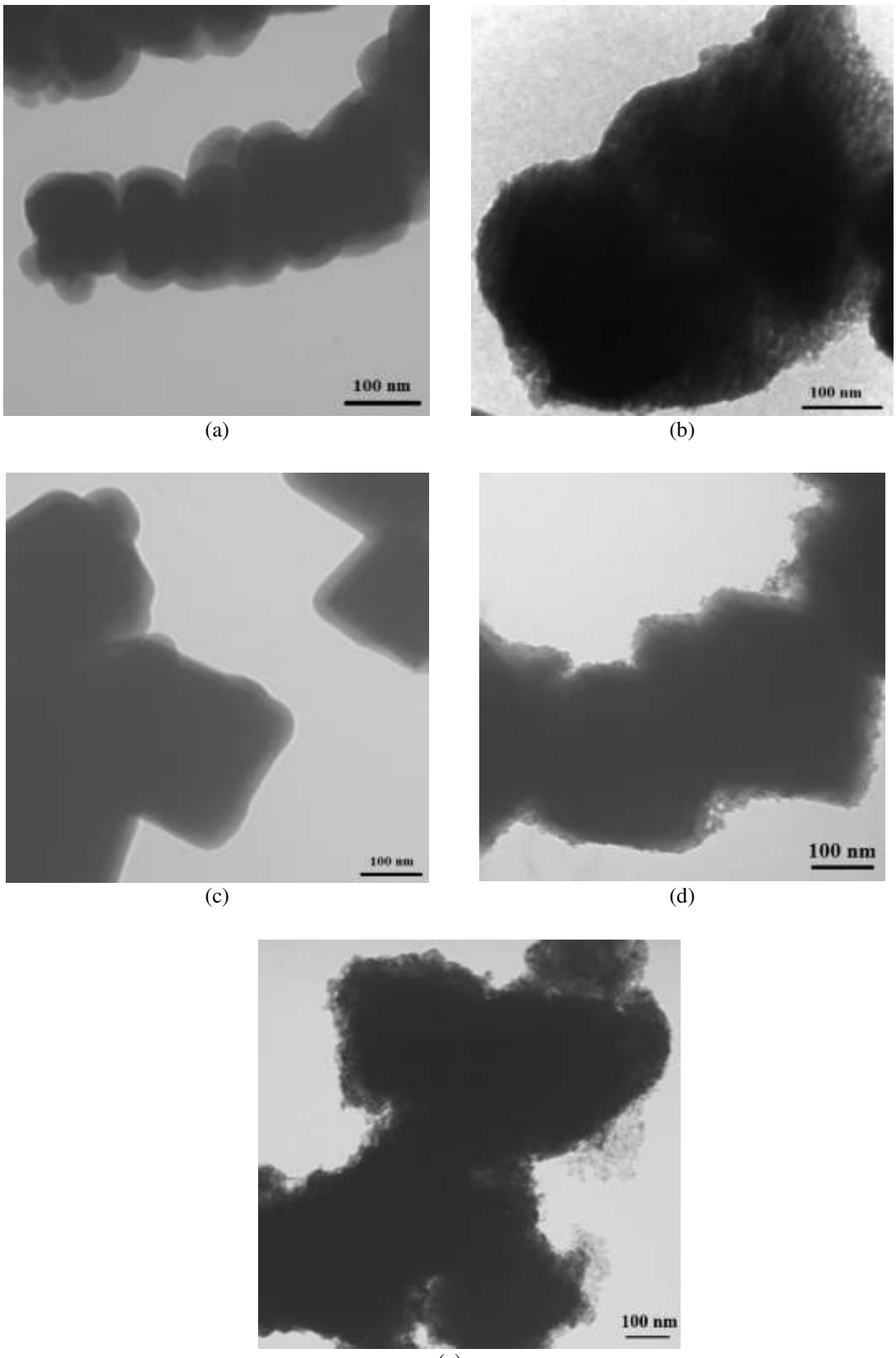

(a) (b)

(c) (d)

(e)

Fig. 4 TEM micrographs of a) $SrFe_{12}O_{19}/SiO_2$, b) $SrFe_{12}O_{19}/SiO_2/TiO_2$, c) Fe_3O_4/SiO_2, d) $Fe_3O_4/SiO_2/ZnO$ and e) $Fe_3O_4/SiO_2/TiO_2$ composites

Fig. 5 illustrates the magnetic properties of the various synthesized powders. Fig. 5 (a) compares the magnetic properties of Fe_3O_4 and $SrFe_{12}O_{19}$ core particles. As can be seen, the fabricated Fe_3O_4 soft magnetic particles show clear ferromagnetism hysteresis due to the narrow hysteresis loop, while the wide hysteresis curve as a typical characteristic for ferrimagnetism is clearly observed for the $SrFe_{12}O_{19}$ particles [35]. Furthermore, the saturation magnetization for Fe_3O_4 powder is more than that for $SrFe_{12}O_{19}$ powder.

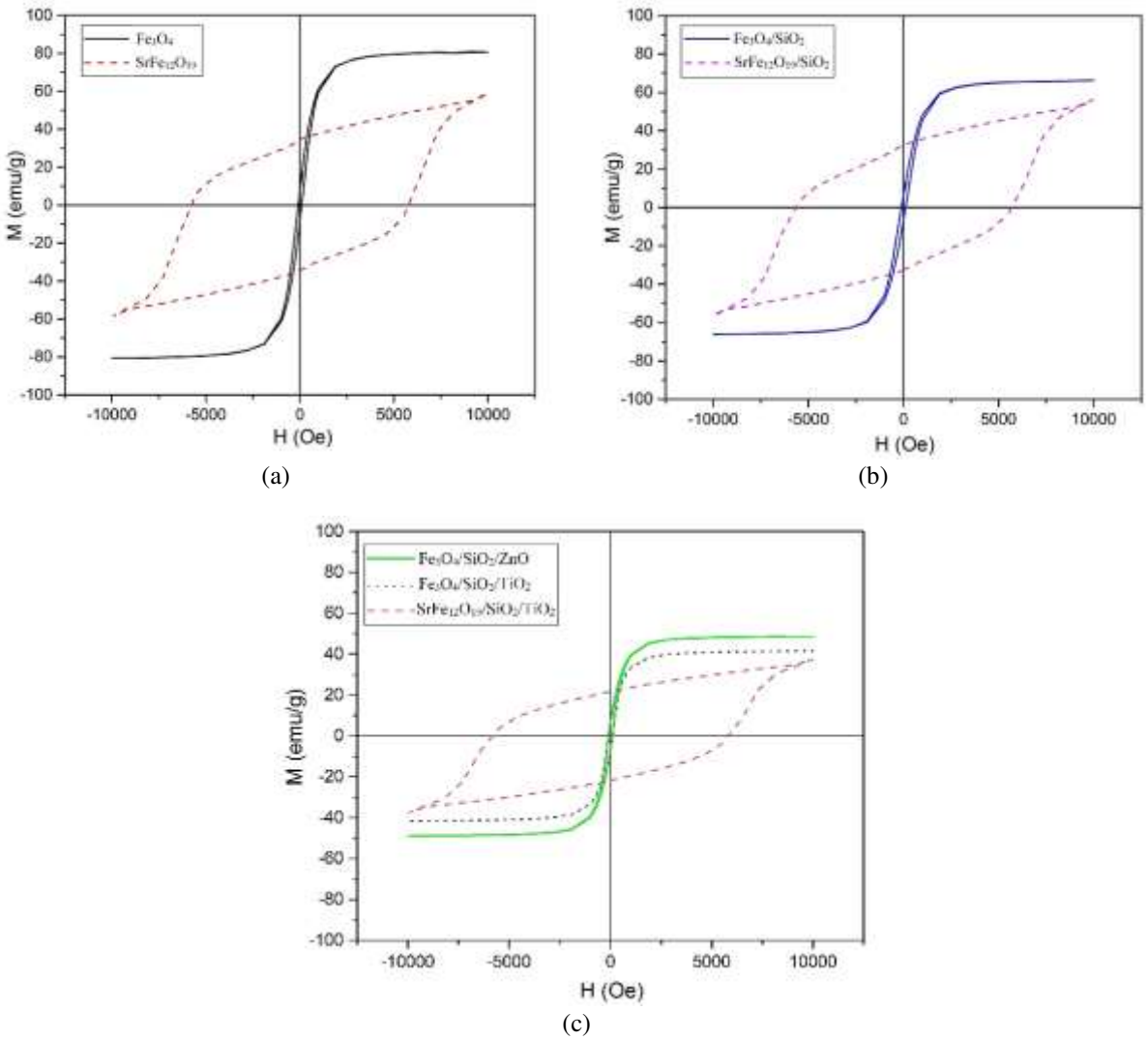

Fig. 5 Magnetic loops for a) synthesized magnetic cores, b) $SrFe_{12}O_{19}/SiO_2$ and Fe_3O_4/SiO_2 composites, c) $Fe_3O_4/SiO_2/TiO_2$, $Fe_3O_4/SiO_2/ZnO$ and $SrFe_{12}O_{19}/SiO_2/TiO_2$ photo-catalytic composites at room-temperature

The magnetic characteristics of Fe_3O_4/SiO_2, $SrFe_{12}O_{19}/SiO_2$, $Fe_3O_4/SiO_2/ZnO$, $Fe_3O_4/SiO_2/TiO_2$ and $SrFe_{12}O_{19}/SiO_2/TiO_2$ are represented in Figs. 5 (b) and (c). The reduction of the magnetic properties of the as-prepared core-shell nanostructures confirms the coating of silica and photo-catalytic shells [36, 37]. The saturation magnetization of the $Fe_3O_4/SiO_2/ZnO$, $Fe_3O_4/SiO_2/TiO_2$ and $SrFe_{12}O_{19}/SiO_2/TiO_2$ photo-catalytic nanostructures was 49 emu/g, 41.5 emu/g and 33 emu/g, respectively. Less saturation magnetization of $SrFe_{12}O_{19}/SiO_2/TiO_2$ photo-catalyst could be due to less agglomeration. Although the coating process causes some degree of agglomeration in particles (as shown in Fig. 2(b-c-d and f-g)), however visual examination of $SrFe_{12}O_{19}/SiO_2/TiO_2$ powders also confirms comparatively less agglomeration of $SrFe_{12}O_{19}/SiO_2/TiO_2$ powders.

Fig. 6 shows the changes in absorption spectra of methylene blue dye in the presence of $Fe_3O_4/SiO_2/ZnO$, $Fe_3O_4/SiO_2/TiO_2$ and $SrFe_{12}O_{19}/SiO_2/TiO_2$ photo-catalytic composite powders after various times of 10, 30, 90 and 180 min of UV light exposure. The maximum absorption of methylene blue solution is at 664 nm wavelength [27].

By examination of absorption changes at the maximum wavelength, the destruction percentage of methylene blue dye was obtained using the following equation [38]:

$$D(\%) = \left(\frac{A_o - A_t}{A_o} \right) \times 100 \qquad (3)$$

where D is the percentage of degradation, A_0 and A_t are absorbance intensity in wavelength of 664 nm at times of 0 and t, respectively.

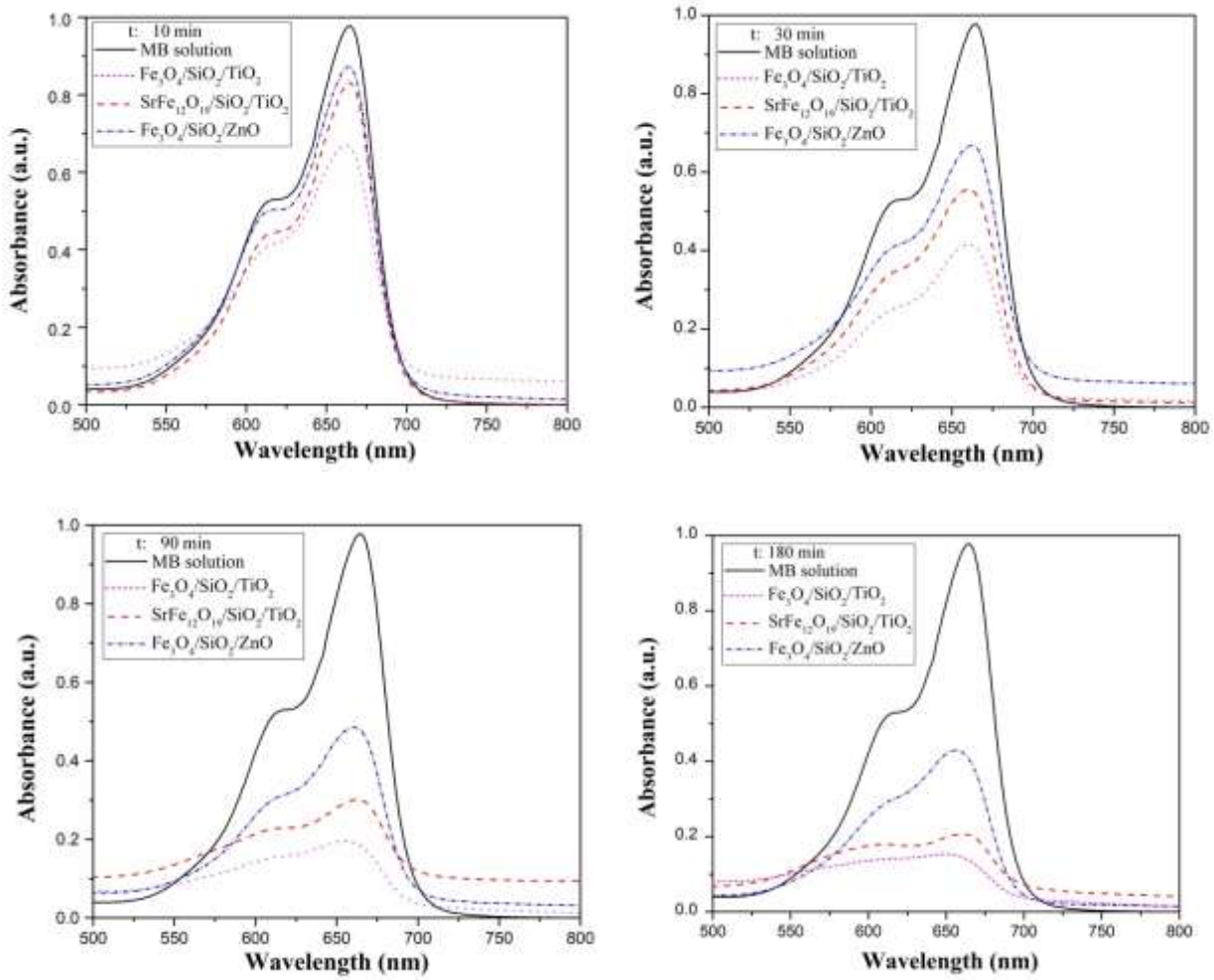

Fig. 6 Absorbance spectra of MB dye solution in the presence of photo-catalytic powders of $Fe_3O_4/SiO_2/TiO_2$, $SrFe_{12}O_{19}/SiO_2/TiO_2$ and $Fe_3O_4/SiO_2/ZnO$ after different UV-irradiation times

Fig. 7 compares the effect of the addition of $Fe_3O_4/SiO_2/TiO_2$, $Fe_3O_4/SiO_2/ZnO$ and $SrFe_{12}O_{19}/SiO_2/TiO_2$ photo-catalytic powders on the degradation of methylene blue dye at different times. Destruction percentages under UV light due to the addition of $Fe_3O_4/SiO_2/TiO_2$ photo-catalytic powder to the MB solution (50 mg/l) for various times of 10, 30, 90, and 180 min, were 32%, 58%, 80% and 84%, respectively, and destruction percentages in the presence of $SrFe_{12}O_{19}/SiO_2/TiO_2$ photo-catalytic powder for similar times were 16%, 44%, 69% and 80%, respectively, whereas destruction percentages for $Fe_3O_4/SiO_2/ZnO$ photo-catalytic powder at similar times were 11%, 32%, 51% and 58%, respectively. The degradation of methylene blue dye confirms the presence and coating of photo-catalytic shells. Maximum degradation of methylene blue dye obtained 84% for $Fe_3O_4/SiO_2/TiO_2$ composite under UV light exposure of 180 min. The higher photo-catalytic efficiency of the $Fe_3O_4/SiO_2/TiO_2$

and $SrFe_{12}O_{19}/SiO_2/TiO_2$ composites could be due to the thickening of the TiO_2 shell than the ZnO shell. The better photo-catalytic properties of these composites relative to $Fe_3O_4/SiO_2/ZnO$ could also be attributed to the smaller band gap of TiO_2 (3.2 ev) than that of ZnO (3.37 ev) [16, 27]. On the other hand, decreasing the amount of agglomeration is effective in improving photo-catalytic activity. The less agglomeration of photo-catalytic particles cause increased contact surface with the pollutants and consequently the photo-catalytic efficiency increases. Therefore, less agglomeration of $SrFe_{12}O_{19}/SiO_2/TiO_2$ powders, as mentioned earlier, could be an effective parameter in increasing its photo-catalytic efficiency. On the other hand, increasing the surface to volume ratio improves catalytic activity [39]. It is well known that the surface to volume ratio of the cubic shape is higher than that of other shapes such as dodecahedron, octahedron, sphere and icosahedron [39, 40]. Therefore, the photocatalytic properties of the $Fe_3O_4/SiO_2/TiO_2$ composite are slightly better than those of $SrFe_{12}O_{19}/SiO_2/TiO_2$ composite due to the cubic shape of its magnetic core. Fig. 7 also indicates a slight photo-catalytic degradation of MB in the presence of Fe_3O_4/SiO_2 and $SrFe_{12}O_{19}/SiO_2$ composites. The partial bleaching of methylene blue molecules under UV light and the adsorption of methylene blue molecules to the surface of the composite powders resulted in minor degradation of methylene blue dye [41].

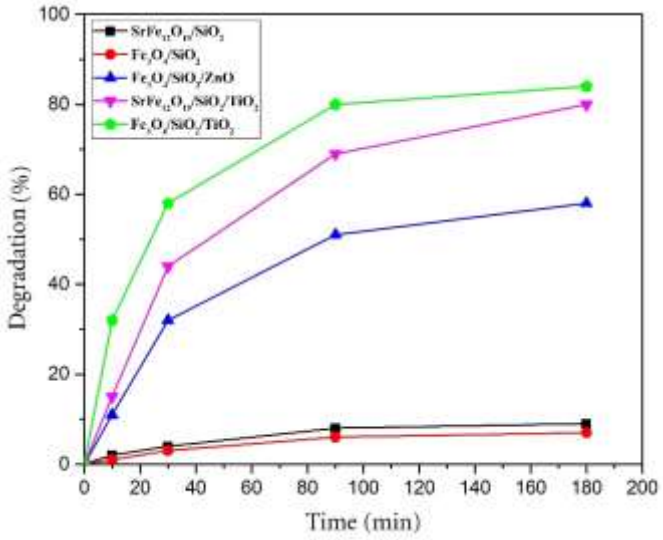

Fig. 7 Comparison of MB dye destruction in the presence of $Fe_3O_4/SiO_2/TiO_2$, $SrFe_{12}O_{19}/SiO_2/TiO_2$, $Fe_3O_4/SiO_2/ZnO$, $SrFe_{12}O_{19}/SiO_2$ and Fe_3O_4/SiO_2 composites after different times of UV-irradiation

To evaluate the recovery of photo-catalytic properties of $Fe_3O_4/SiO_2/TiO_2$, $Fe_3O_4/SiO_2/ZnO$ and $SrFe_{12}O_{19}/SiO_2/TiO_2$ powders, three consecutive cycles of decomposition of methylene blue were studied. Fig. 8 compares methylene blue destruction by $Fe_3O_4/SiO_2/TiO_2$, $Fe_3O_4/SiO_2/ZnO$ and $SrFe_{12}O_{19}/SiO_2/TiO_2$ composites at three cycles. By increasing reuse time, the photo-catalytic activity of three composites has decreased, which can be due to the formation of organic intermediate products and accumulation of them in the cavity sites and the surface of the catalysts [42]. However, the removal efficiency by $Fe_3O_4/SiO_2/TiO_2$, $Fe_3O_4/SiO_2/ZnO$ and $SrFe_{12}O_{19}/SiO_2/TiO_2$ composites was approximately remained 94, 91 and 95 percent of that of the first operation, respectively, after three consecutive cycles. The results suggest that the recovered powders have relatively good photo-catalytic activity. Hence, they could be retrieved with an external magnetic field and re-used.

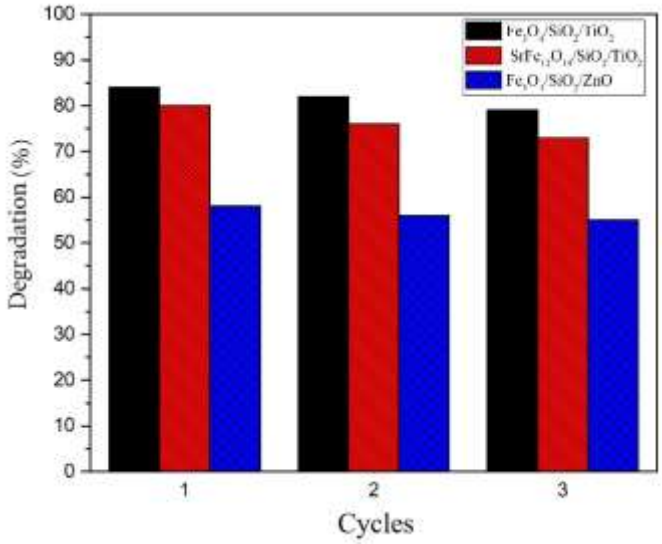

Fig. 8 Sequential cycles of decomposition of methylene blue using $Fe_3O_4/SiO_2/TiO_2$, $SrFe_{12}O_{19}/SiO_2/TiO_2$ and $Fe_3O_4/SiO_2/ZnO$ composites

Fig. 9 represents the kinetics of discoloration of MB dye by photo-catalytic powders of $Fe_3O_4/SiO_2/TiO_2$, $Fe_3O_4/SiO_2/ZnO$ and $SrFe_{12}O_{19}/SiO_2/TiO_2$ at two wavelengths of 617 and 664 nm. The photo-catalytic reaction is described by the $LnC_0/C=K_{app}t$ formula that k_{app} is the apparent rate constant of photo-catalytic degradation [43]. The goodness of linear fit on data is evaluated by employing the R^2 value as the correlation coefficient factor. The k_{app} at the wavelength of 664 nm for three composites is more than that at 617 nm wavelength, which is in accordance with Fig.

6 that showed more absorption intensity at 664 nm relative to that at 617 nm [44]. By comparison of destruction kinetics for $Fe_3O_4/SiO_2/TiO_2$, $SrFe_{12}O_{19}/SiO_2/TiO_2$ and $Fe_3O_4/SiO_2/ZnO$ composites, it confirms that the photo-catalytic efficiencies of $Fe_3O_4/SiO_2/TiO_2$ and $SrFe_{12}O_{19}/SiO_2/TiO_2$ composites are larger than that of $Fe_3O_4/SiO_2/ZnO$ composite.

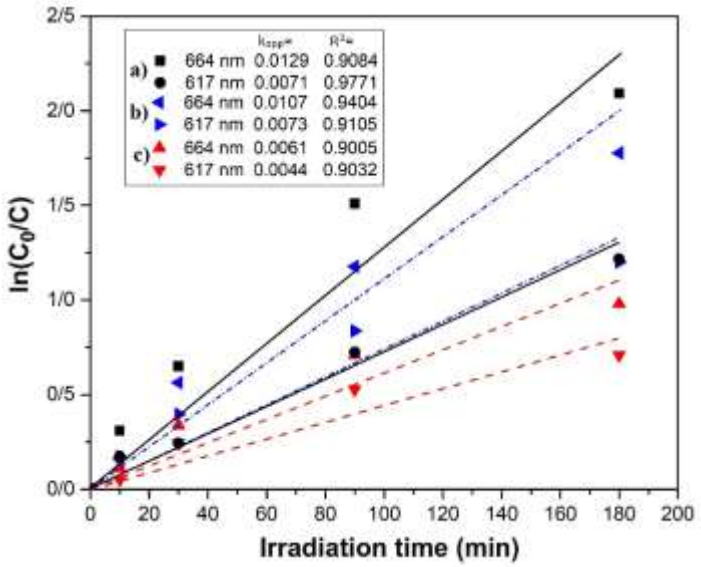

Fig. 9 Kinetics of MB dye disappearance in the presence of a) $Fe_3O_4/SiO_2/TiO_2$, b) $SrFe_{12}O_{19}/SiO_2/TiO_2$ and c) $Fe_3O_4/SiO_2/ZnO$ powders and under different wavelengths

4. Conclusions

The Fe_3O_4 particles as soft magnetic cores of core-shell structured composites were successfully synthesized by the carbon reduction method, and the $SrFe_{12}O_{19}$ particles as hard magnetic cores were prepared by a co-precipitation method in water-ethanol media. The coating of silica shells was performed on $SrFe_{12}O_{19}$ and Fe_3O_4 magnetic particles using the hydrolysis and condensation of TEOS precursor at room temperature. The photo-catalytic composites of $Fe_3O_4/SiO_2/TiO_2$, $SrFe_{12}O_{19}/SiO_2/TiO_2$ and $Fe_3O_4/SiO_2/ZnO$ were successfully prepared using titanium n-butoxide (TNBT) or zinc nitrate hexahydrate precursors.

Microscopy characterization by FESEM and TEM indicated that all synthesized core/ /shell/shell composites were covered with a layer composed of photo-catalyst. However, the TiO_2 photo-catalytic shells were thicker and the coating process was

done at the lower time, and consequently coating process was easier compared to the formation of the ZnO photo-catalytic shells. The saturation magnetization of $Fe_3O_4/SiO_2/ZnO$, $Fe_3O_4/SiO_2/TiO_2$ and $SrFe_{12}O_{19}/SiO_2/TiO_2$ composites with core/shell/shell structure was 49 emu/g, 41.5 emu/g and 33 emu/g, respectively. Less saturation magnetization of $SrFe_{12}O_{19}/SiO_2/TiO_2$ photo-catalyst could be due to less agglomeration and the nature of core material; however, it resulted in an acceptable recovery by magnetic separation.

Photo-catalytic efficiencies of $Fe_3O_4/SiO_2/ZnO$, $SrFe_{12}O_{19}/SiO_2/TiO_2$ and $Fe_3O_4/SiO_2/TiO_2$ composite materials were obtained as 58%, 80% and 84% by the considering degradation of methylene blue dye. It was found that the photo-catalytic properties of titania coating in the composite with core/shell/shell structure can be improved via increasing surface to volume ratio by using the cubic-shape core particles. Thus, the as-prepared $Fe_3O_4/SiO_2/TiO_2$ composite powder has optimum photo-catalytic efficiency compared with $SrFe_{12}O_{19}/SiO_2/TiO_2$ and $Fe_3O_4/SiO_2/ZnO$ composites. However, as seen in sequential cycles of the destruction of MB, all synthesized photo-catalytic composites were nearly well recovered.

Acknowledgment

The authors would like to thank Iran National Science Foundation (INSF) and also the Biosphere Technology Company for full financial support of this joint research project. This work has been carried out under the contract number of 94/sad/42699 on 9/11/2015. Some experiments were performed in the Environmental Laboratory of the Biosphere Technology Company.

References

1. G. Li, Z. Wang, M. Yu, Z. Quan and J. Lin, Fabrication and optical properties of core–shell structured spherical SiO_2@$GdVO_4$: Eu^{3+} phosphors via sol–gel process. *Journal of Solid State Chemistry*, Vol. 179, pp. 2698-2706 (2006)

2. G. Liu, G. Hong and D. Sun, Synthesis and characterization of SiO_2/Gd_2O_3: Eu core–shell luminescent materials. *Journal of Colloid and Interface Science*, Vol. 278, pp. 133-138 (2004)

3. F. Farahbakhsh, M. Ahmadi, S. H. Hekmatara, M. Sabet and E. Heydari-Bafrooei, Improvement of photocatalyst properties of magnetic NPs by new anionic surfactant. *Materials Chemistry and Physics*, Vol. 224, pp. 279-285 (2019)

4. S. Chen, M. Cheng, Y. Lang, C. Tian, H. Wei and C.-A. Wang, Preparation and characterization of monodispersed spherical Fe_2O_3@SiO_2 reddish pigments with core–shell structure. *Journal of Advanced Ceramics*, Vol. 8, pp. 39-46 (2019)

5. S. Kalele, S. Gosavi, J. Urban and S. Kulkarni, Nanoshell particles: synthesis, properties and applications. *Current Science*, pp. 1038-1052 (2006)

6. C. Berberidou, I. Poulios, N. Xekoukoulotakis and D. Mantzavinos, Sonolytic, photocatalytic and sonophotocatalytic degradation of malachite green in aqueous solutions. *Applied Catalysis B: Environmental*, Vol. 74, pp. 63-72 (2007)

7. T. Sauer, G. C. Neto, H. Jose and R. Moreira, Kinetics of photocatalytic degradation of reactive dyes in a TiO_2 slurry reactor. *Journal of Photochemistry and Photobiology A: Chemistry*, Vol. 149, pp. 147-154 (2002)

8. B. Cui, H. Peng, H. Xia, X. Guo and H. Guo, Magnetically recoverable core–shell nanocomposites γ-Fe_2O_3@SiO_2@TiO_2–Ag with enhanced photocatalytic activity and antibacterial activity. *Separation and Purification Technology*, Vol. 103, pp. 251-257 (2013)

9. Y. Chi, Q. Yuan, Y. Li, L. Zhao, N. Li, X. Li and W. Yan, Magnetically separable Fe_3O_4@SiO_2@TiO_2-Ag microspheres with well-designed nanostructure and enhanced photocatalytic activity. *Journal of Hazardous Materials*, Vol. 262, pp. 404-411 (2013)

10. D. Wang, D. Han, J. Yang, J. Wang, X. Li and H. Song, Controlled preparation of superparamagnetic Fe_3O_4@SiO_2@ZnO-Au core-shell photocatalyst with superior activity: RhB degradation and working mechanism. *Powder Technology*, Vol. 327, pp. 489-499 (2018)

11. S.-w. Lee, J. Drwiega, D. Mazyck, C.-Y. Wu and W. M. Sigmund, Synthesis and characterization of hard magnetic composite photocatalyst—Barium ferrite/silica/titania. *Materials Chemistry and Physics*, Vol. 96, pp. 483-488 (2006)

12. S. Watson, D. Beydoun and R. Amal, Synthesis of a novel magnetic photocatalyst by direct deposition of nanosized TiO_2 crystals onto a magnetic core. *Journal of Photochemistry and Photobiology A: Chemistry*, Vol. 148, pp. 303-313 (2002)

13. D. Wang, D. Han, Z. Shi, J. Wang, J. Yang, X. Li and H. Song, Optimized design of three-dimensional multi-shell Fe_3O_4/SiO_2/ZnO/ZnSe microspheres with type II heterostructure for photocatalytic applications. *Applied Catalysis B: Environmental*, Vol. 227, pp. 61-69 (2018)

14. D. Beydoun, R. Amal, G. K.-C. Low and S. McEvoy, Novel photocatalyst: titania-coated magnetite. Activity and photodissolution. *The Journal of Physical Chemistry B*, Vol. 104, pp. 4387-4396 (2000)

15. Y. Gao, B. Chen, H. Li and Y. Ma, Preparation and characterization of a magnetically separated photocatalyst and its catalytic properties. *Materials Chemistry and Physics*, Vol. 80, pp. 348-355 (2003)

16. J. Wang, J. Yang, X. Li, B. Wei, D. Wang, H. Song, H. Zhai and X. Li, Synthesis of Fe_3O_4@SiO_2@ZnO–Ag core–shell microspheres for the repeated photocatalytic degradation of rhodamine B under UV irradiation. *Journal of Molecular Catalysis A: Chemical*, Vol. 406, pp. 97-105 (2015)

17. R. Fu, X. Jin, J. Liang, W. Zheng, J. Zhuang and W. Yang, Preparation of nearly monodispersed Fe_3O_4/SiO_2 composite particles from aggregates of Fe3O4 nanoparticles. *Journal of Materials Chemistry*, Vol. 21, pp. 15352-15356 (2011)

18. Y. Wang, X. Peng, J. Shi, X. Tang, J. Jiang and W. Liu, Highly selective fluorescent chemosensor for Zn^{2+} derived from inorganic-organic hybrid magnetic core/shell Fe_3O_4@ SiO_2 nanoparticles. *Nanoscale Research Letters*, Vol. 7, pp. 86 (2012)

19. C. Hui, C. Shen, J. Tian, L. Bao, H. Ding, C. Li, Y. Tian, X. Shi and H.-J. Gao, Core-shell Fe_3O_4@SiO_2 nanoparticles synthesized with well-dispersed hydrophilic Fe_3O_4 seeds. *Nanoscale*, Vol. 3, pp. 701-705 (2011)

20. D. H. Everett, *Basic Principles of Colloid Science*, Royal Society of Chemistry, 1988.

21. F. Bavarsiha, M. Rajabi and M. Montazeri-Pour, Synthesis of $SrFe_{12}O_{19}$/SiO_2/TiO_2 composites with core/shell/shell nano-structure and evaluation of their photo-catalytic efficiency for degradation of methylene blue. *Journal of Materials Science: Materials in Electronics*, Vol. 29, pp. 1877–1887 (2018)

22. M. Ye, Q. Zhang, Y. Hu, J. Ge, Z. Lu, L. He, Z. Chen and Y. Yin, Magnetically recoverable core–shell nanocomposites with enhanced photocatalytic activity. *Chemistry-A European Journal*, Vol. 16, pp. 6243-6250 (2010)

23. Q. Zhang, L.-B. Gao, J.-Y. Li, Z.-B. Guo, Z.-Y. Hai, Y.-T. Xing and C.-Y. Xue, Synthesis of magnetic carrier sub-microparticles with high stability through carbon reduction and solation coating methods. *Rare Metals*, Vol. 35, pp. 870-873 (2016)

24. M. Montazeri-Pour and A. Ataie, Synthesis of nanocrystalline barium ferrite in ethanol/water media. *Journal of Materials Science & Technology*, Vol. 25, pp. 465 (2009)

25. A. Ataie and M. Montazeri-Pour, Formation mechanism of $BaFe_{12}O_{19}$ nanoparticles processed via wet chemical route using mixed solvent. *International Journal of Nanoscience*, Vol. 10, pp. 1083-1086 (2011)

26. J.-R. Fu, J. Zheng, W.-J. Fang, C. Chen, C. Cheng, R.-W. Yan, S.-G. Huang and C.-C. Wang, Synthesis of porous magnetic Fe_3O_4/Fe@ ZnO core–shell heterostructure with superior capability for water treatment. *Journal of Alloys and Compounds*, Vol. 650, pp. 463-469 (2015)

27. X. Huang, G. Wang, M. Yang, W. Guo and H. Gao, Synthesis of polyaniline-modified $Fe_3O_4/SiO_2/TiO_2$ composite microspheres and their photocatalytic application. *Materials Letters*, Vol. 65, pp. 2887-2890 (2011)

28. J. Li, L. Gao, Q. Zhang, R. Feng, H. Xu, J. Wang, D. Sun and C. Xue, Photocatalytic property of $Fe_3O_4/SiO_2/TiO_2$ core-shell nanoparticle with different functional layer thicknesses. *Journal of Nanomaterials*, Vol. 2014, pp. 2 (2014)

29. Y. Wang, D. Sun, G. Liu and W. Jiang, Synthesis of Fe_3O_4@ SiO_2@ ZnO core–shell structured microspheres and microwave absorption properties. *Advanced Powder Technology*, Vol. 26, pp. 1537-1543 (2015)

30. V. Belessi, D. Lambropoulou, I. Konstantinou, R. Zboril, J. Tucek, D. Jancik, T. Albanis and D. Petridis, Structure and photocatalytic performance of magnetically separable titania photocatalysts for the degradation of propachlor. *Applied Catalysis B: Environmental*, Vol. 87, pp. 181-189 (2009)

31. Y.-H. Deng, C.-C. Wang, J.-H. Hu, W.-L. Yang and S.-K. Fu, Investigation of formation of silica-coated magnetite nanoparticles via sol–gel approach. *Colloids and Surfaces A: Physicochemical and Engineering Aspects*, Vol. 262, pp. 87-93 (2005)

32. Q. Yuan, N. Li, W. Geng, Y. Chi and X. Li, Preparation of magnetically recoverable Fe_3O_4@ SiO_2@ meso-TiO_2 nanocomposites with enhanced photocatalytic ability. *Materials Research Bulletin*, Vol. 47, pp. 2396-2402 (2012)

33. L. Guo, K. Liang, K. Marcus, Z. Li, L. Zhou, P. D. Mani, H. Chen, C. Shen, Y. Dong and L. Zhai, Enhanced photoelectrocatalytic reduction of oxygen using Au@TiO_2 plasmonic film. *ACS Applied Materials & Interfaces*, Vol. 8, pp. 34970-34977 (2016)

34. V. Tizjang, M. Montazeri-Pour, M. Rajabi, M. Kari and S. Moghadas, Surface modification of sol–gel synthesized TiO_2 photo-catalysts for the production of core/shell structured TiO_2–SiO_2 nano-composites with reduced photo-catalytic activity. *Journal of Materials Science: Materials in Electronics*, Vol. 26, pp. 3008-3019 (2015)

35. F. Bavarsiha, M. Montazeri-Pour and M. Rajabi, Effect of non-aqueous media on nano-crystalline $SrFe_{12}O_{19}$ particles produced by co-precipitation with metal chlorides and evaluation of their magnetic and photocatalytic properties. *Journal of Inorganic and Organometallic Polymers and Materials*, Vol. 30, pp. 2386-2396 (2020)

36. Z. Wang, L. Shen and S. Zhu, Synthesis of core-shell Fe_3O_4@SiO_2@TiO_2 microspheres and their application as recyclable photocatalysts. *International Journal of Photoenergy*, Vol. 2012, (2012)

37. F. Parast, M. Montazeri-Pour, M. Rajabi and F. Bavarsiha, Comparison of the structural and photo-catalytic properties of nanostructured Fe_3O_4/TiO_2 core-shell composites

synthesized by ultrasonic and Stöber methods. *Science of Sintering*, Vol. 52, pp. 415-432 (2020)

38. M. Kari, M. Montazeri-Pour, M. Rajabi, V. Tizjang and S. Moghadas, Maximum SiO_2 layer thickness by utilizing polyethylene glycol as the surfactant in synthesis of core/shell structured TiO_2–SiO_2 nano-composites. *Journal of Materials Science: Materials in Electronics*, Vol. 25, pp. 5560-5569 (2014)

39. M. Abbas, B. P. Rao, V. Reddy and C. Kim, Fe_3O_4/TiO_2 core/shell nanocubes: Single-batch surfactantless synthesis, characterization and efficient catalysts for methylene blue degradation. *Ceramics International*, Vol. 40, pp. 11177-11186 (2014)

40. M. Abbas, M. Takahashi and C. Kim, Facile sonochemical synthesis of high-moment magnetite (Fe_3O_4) nanocube. *Journal of Nanoparticle Research*, Vol. 15, pp. 1354 (2013)

41. D. Greene, R. Serrano-Garcia, J. Govan and Y. K. Gun'ko, Synthesis characterization and photocatalytic studies of cobalt ferrite-silica-titania nanocomposites. *Nanomaterials*, Vol. 4, pp. 331-343 (2014)

42. S. Gomez, C. L. Marchena, L. Pizzio and L. Pierella, Preparation and characterization of TiO_2/HZSM-11 zeolite for photodegradation of dichlorvos in aqueous solution. *Journal of Hazardous Materials*, Vol. 258, pp. 19-26 (2013)

43. H. Liu, Z. Jia, S. Ji, Y. Zheng, M. Li and H. Yang, Synthesis of TiO_2/SiO_2@ Fe_3O_4 magnetic microspheres and their properties of photocatalytic degradation dyestuff. *Catalysis Today*, Vol. 175, pp. 293-298 (2011)

44. N. Zhou, L. Polavarapu, N. Gao, Y. Pan, P. Yuan, Q. Wang and Q.-H. Xu, TiO_2 coated Au/Ag nanorods with enhanced photocatalytic activity under visible light irradiation. *Nanoscale*, Vol. 5, pp. 4236-4241 (2013)

Figures

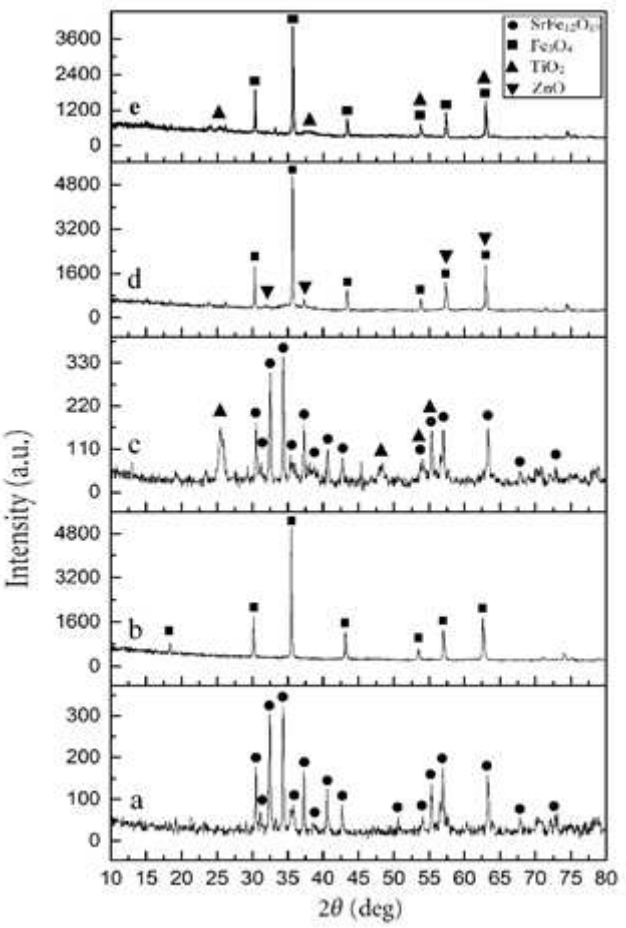

Figure 1

XRD patterns of a) SrFe12O19 powder, b) Fe3O4 powder, c) SrFe12O19/SiO2/TiO2 composites, d) Fe3O4/SiO2/ZnO composites and e) Fe3O4/SiO2/TiO2 composites

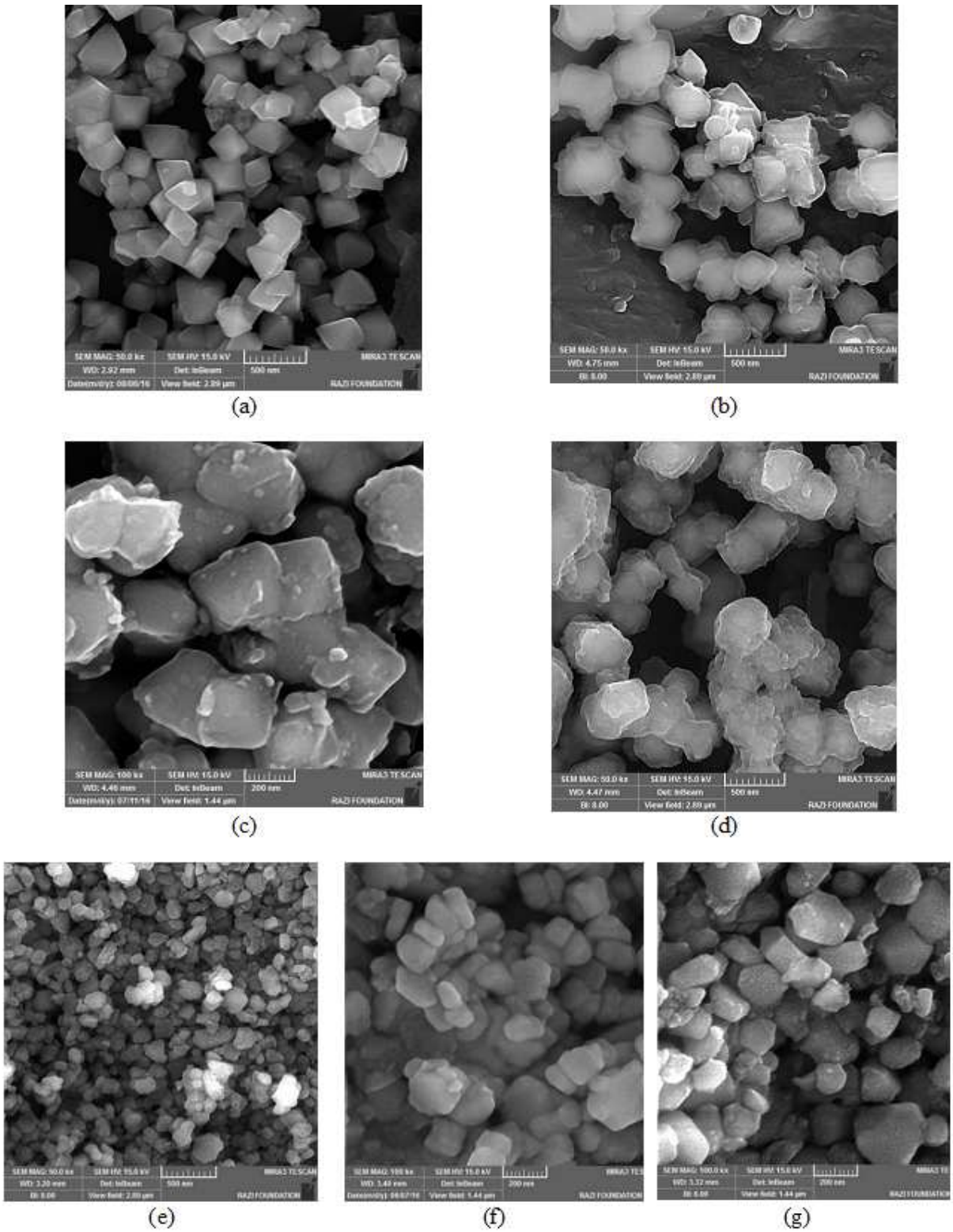

Figure 2

FESEM micrographs of a) Fe3O4 powder, b) Fe3O4/SiO2 composite, c) Fe3O4/SiO2/ZnO composite, d) Fe3O4/SiO2/TiO2 composite, e) SrFe12O19 powder, f) SrFe12O19/SiO2 composite, and g) SrFe12O19/SiO2/TiO2 composite

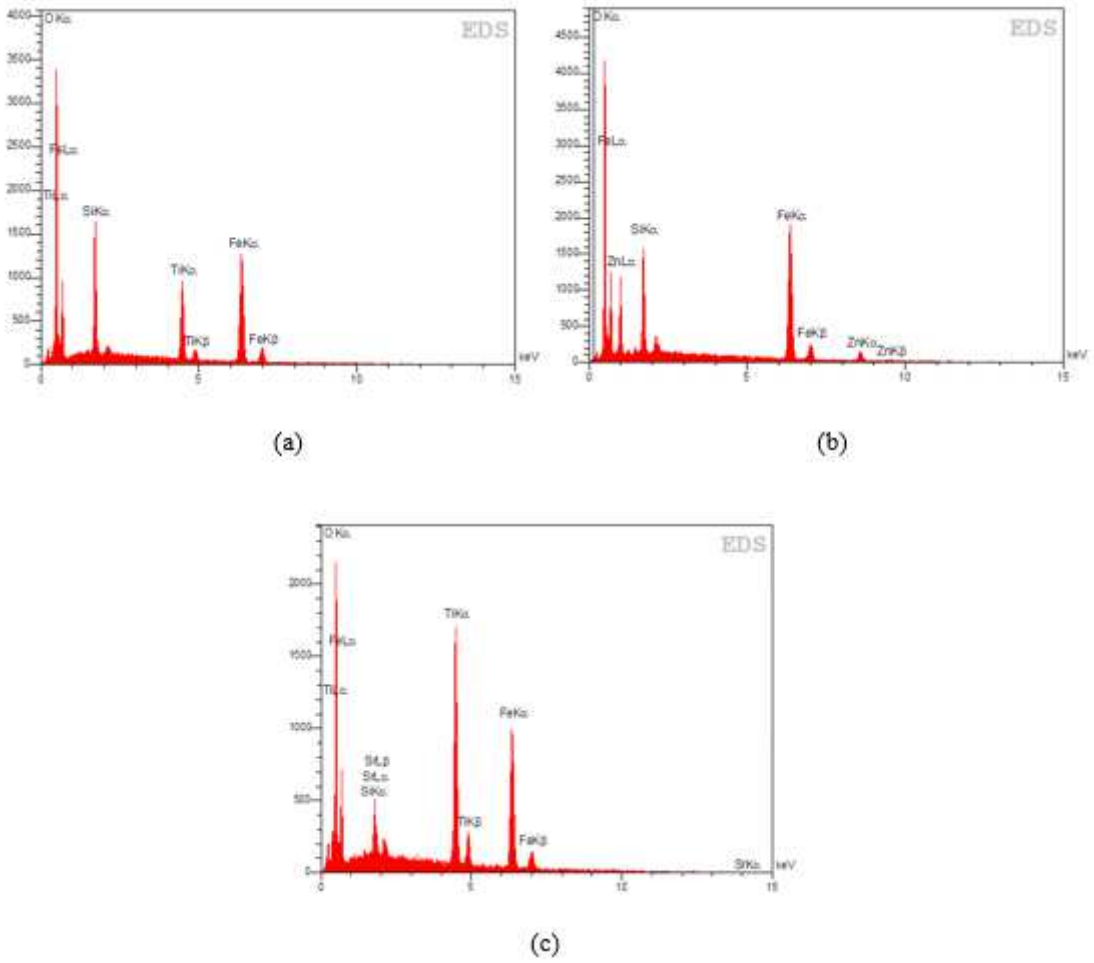

Figure 3

EDS spectra of the a) Fe3O4/SiO2/TiO2, b) Fe3O4/SiO2/ZnO and c) SrFe12O19/SiO2/TiO2 composites

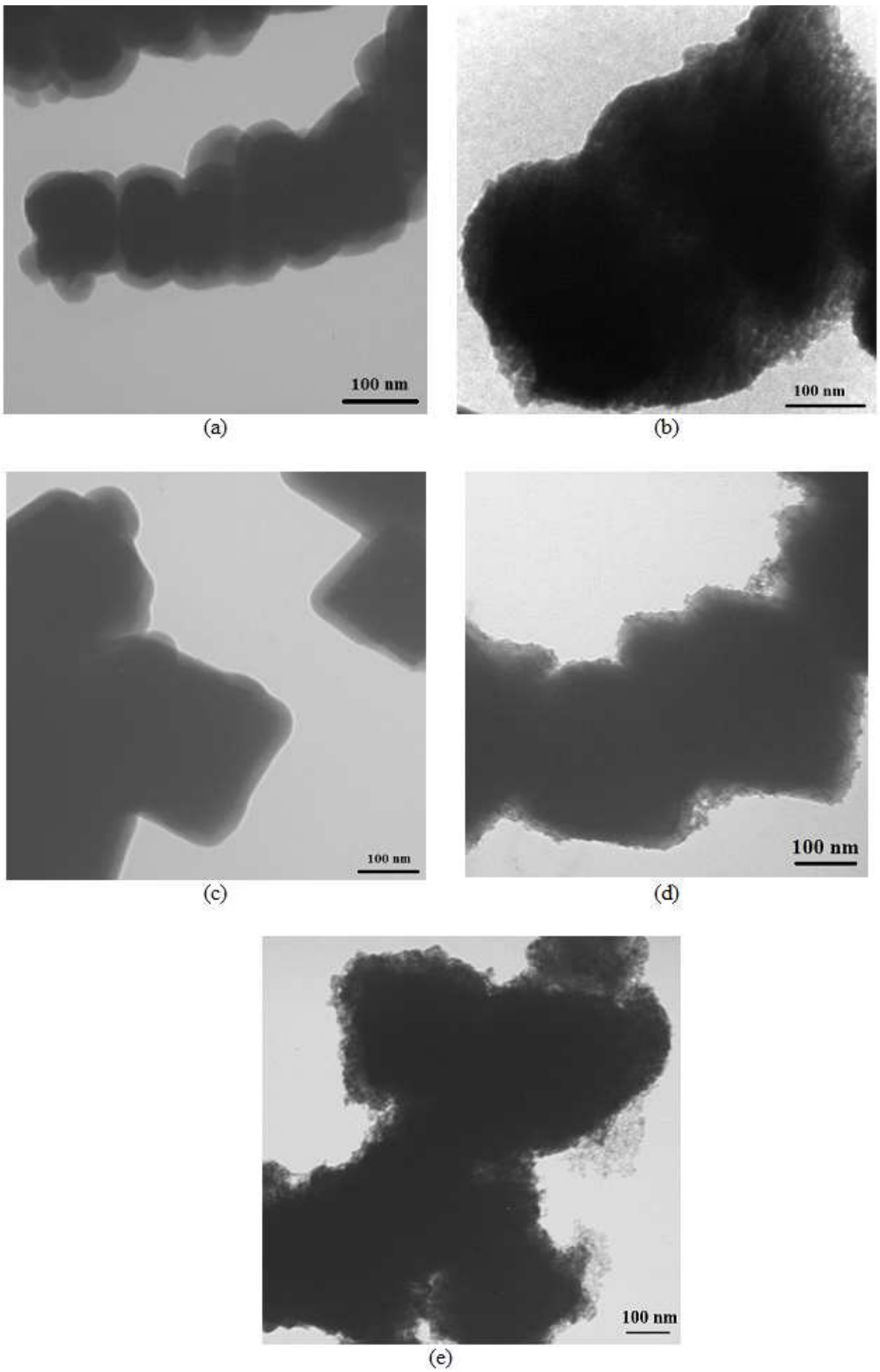

Figure 4

TEM micrographs of a) SrFe12O19/SiO2, b) SrFe12O19/SiO2/TiO2, c) Fe3O4/SiO2, d) Fe3O4/SiO2/ZnO and e) Fe3O4/SiO2/TiO2 composites

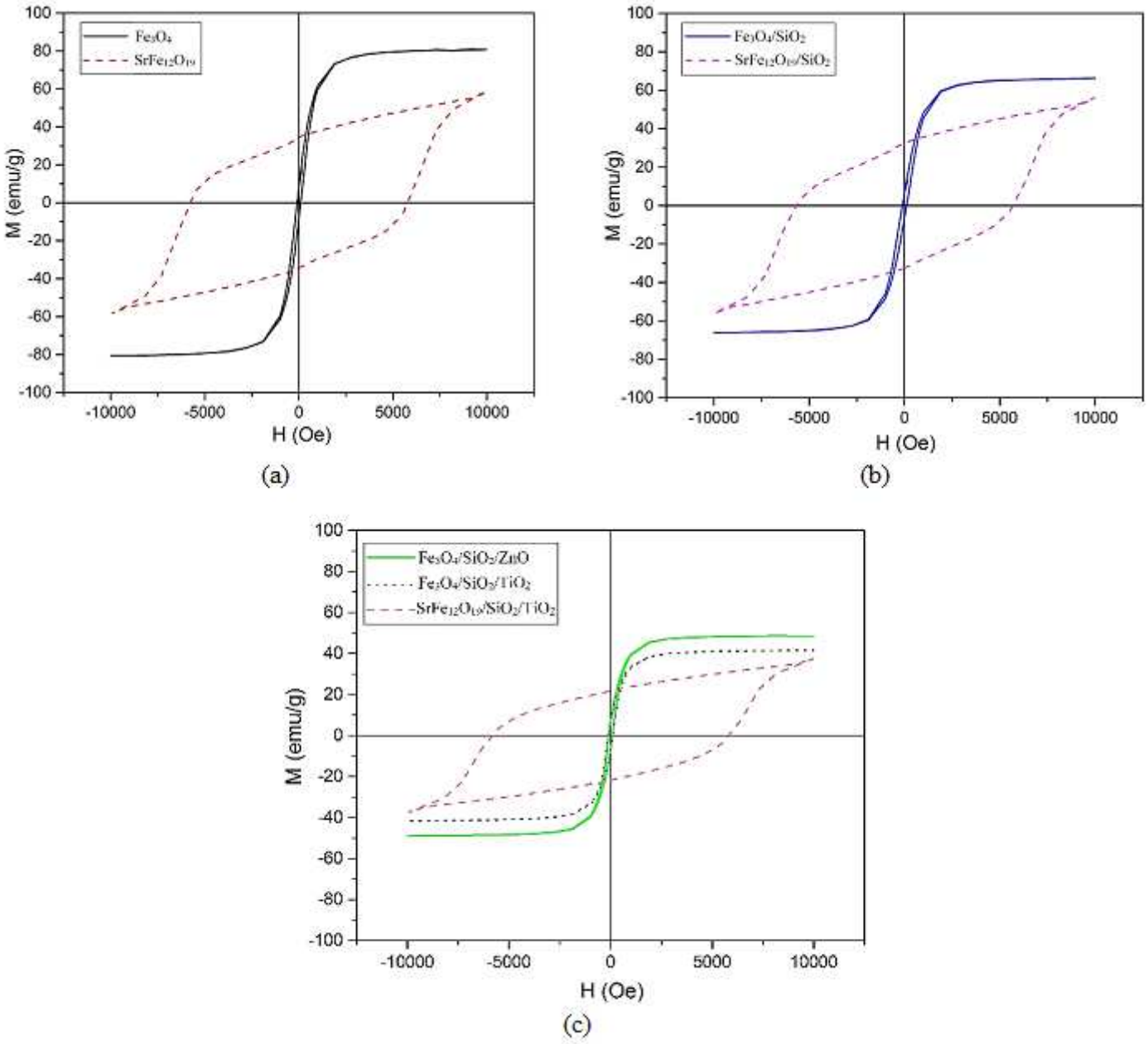

Figure 5

Magnetic loops for a) synthesized magnetic cores, b) SrFe12O19/SiO2 and Fe3O4/SiO2 composites, c) Fe3O4/SiO2/TiO2, Fe3O4/SiO2/ZnO and SrFe12O19/SiO2/TiO2 photo-catalytic composites at room-temperature

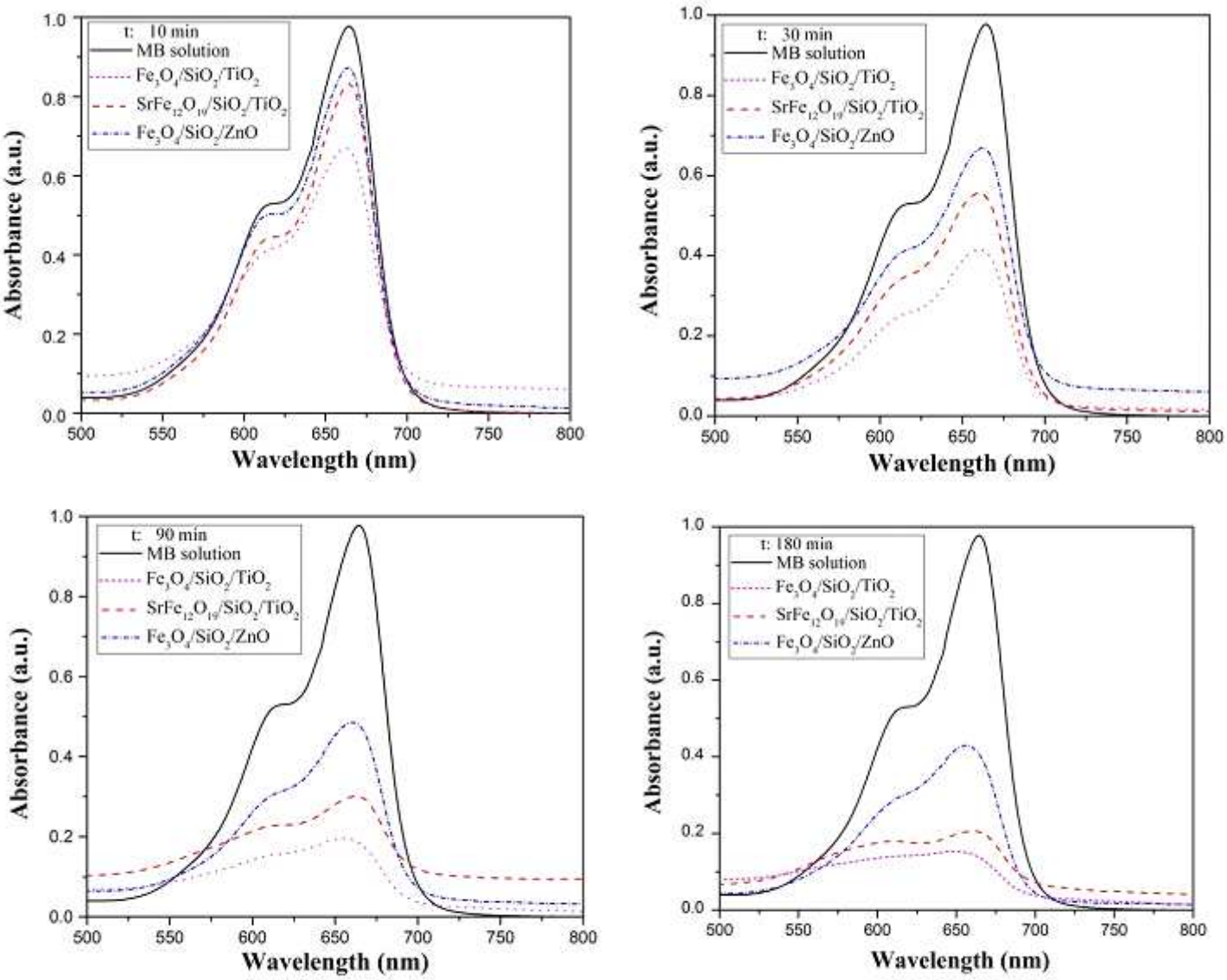

Figure 6

Absorbance spectra of MB dye solution in the presence of photo-catalytic powders of Fe3O4/SiO2/TiO2, SrFe12O19/SiO2/TiO2 and Fe3O4/SiO2/ZnO after different UV-irradiation times

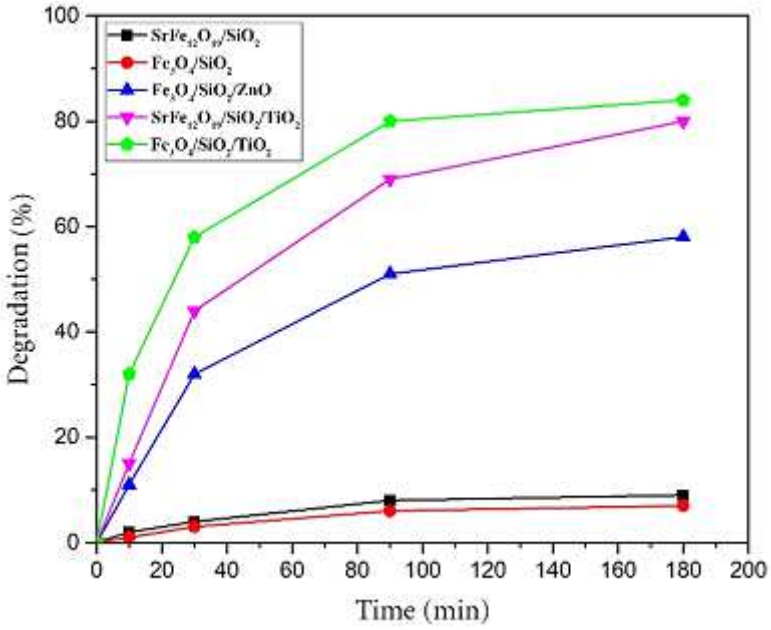

Figure 7

Comparison of MB dye destruction in the presence of Fe3O4/SiO2/TiO2, SrFe12O19/SiO2/TiO2, Fe3O4/SiO2/ZnO, SrFe12O19/SiO2 and Fe3O4/SiO2 composites after different times of UV-irradiation

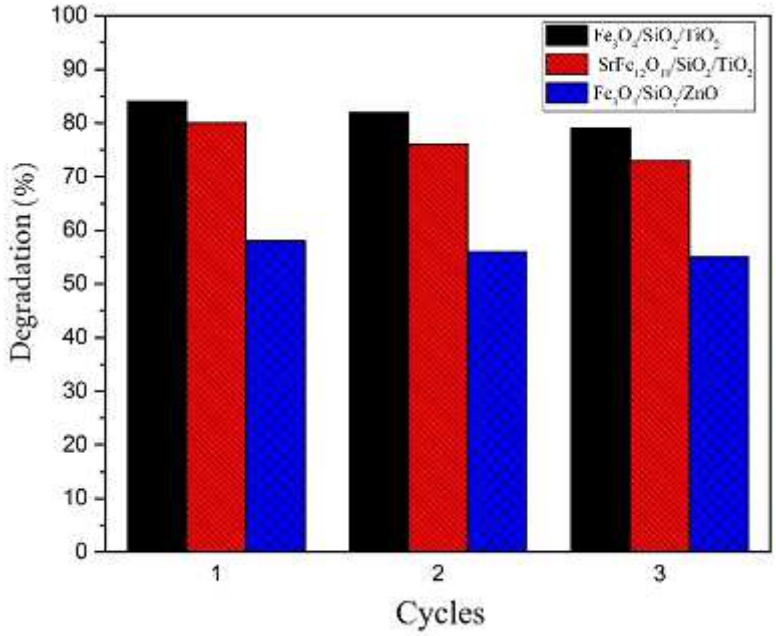

Figure 8

Sequential cycles of decomposition of methylene blue using Fe3O4/SiO2/TiO2, SrFe12O19/SiO2/TiO2 and Fe3O4/SiO2/ZnO composites

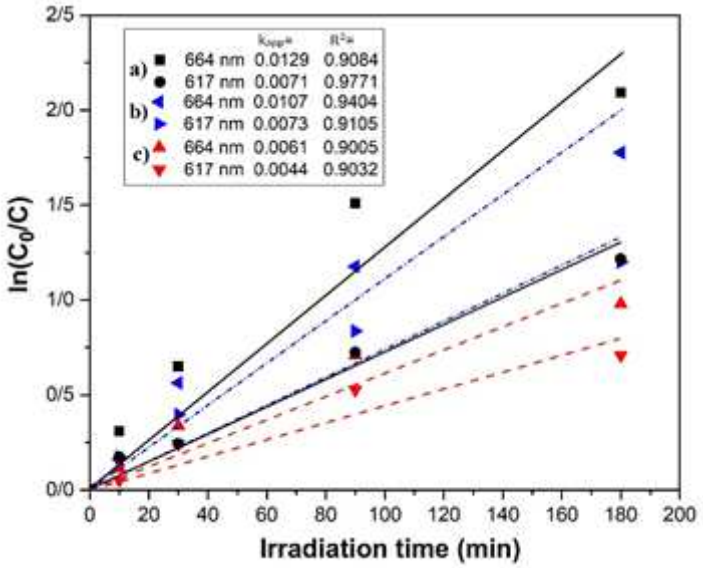

Figure 9

Kinetics of MB dye disappearance in the presence of a) Fe3O4/SiO2/TiO2, b) SrFe12O19/SiO2/TiO2 and c) Fe3O4/SiO2/ZnO powders and under different wavelengths